Limits of Pseudoelasticity in Gold Nanocrystals

K. Anika Harkins¹, Jonas Boettner¹, Lindsey A. Hanson^{1*}

¹Department of Chemistry, Trinity College, Hartford, CT 06106, USA

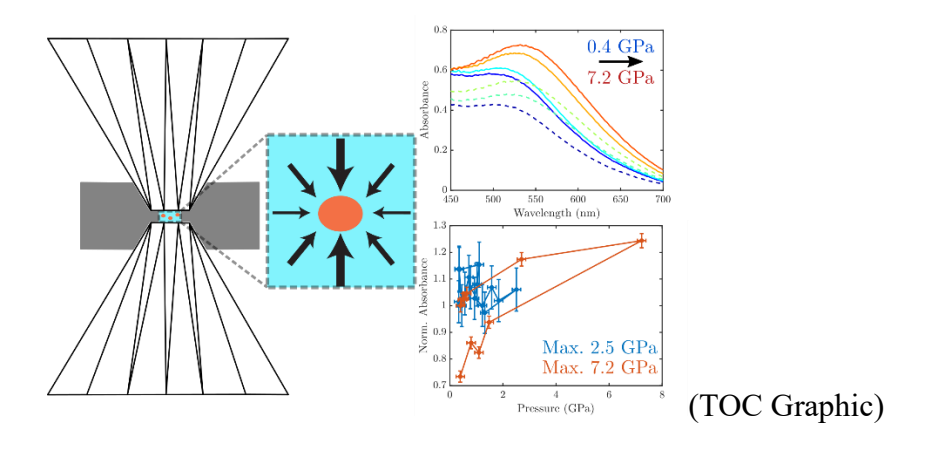
*Corresponding Author: lindsey.hanson@trincoll.edu

KEYWORDS.

Pseudoelasticity, Nanomechanics, Diamond anvil cell, Gold nanoparticles, Plasmonics

ABSTRACT

Pseudoelasticity in metal nanocrystals allows for shape recovery from strains much larger than their bulk counterparts. This fascinating property could be used to engineer self-healing or reconfigurable materials, but to take full advantage of its possibilities a deeper understanding of its mechanism and limitations is needed. For instance, it is unknown whether room-temperature pseudoelasticity can occur in all metal nanocrystals without the introduction of plastic damage. Here we report the use of non-hydrostatic compression of gold nanocrystals in a diamond anvil cell to a range of maximum pressures, up to 11.4 GPa. Optical absorbance spectroscopy of the localized surface plasmon resonance is used to non-invasively monitor changes in particle shape and crystallinity, as indicated by the plasmon resonance peak position and intensity, respectively. We find that while complete shape recovery occurs following compression to all pressures tested, irreversible crystalline defects are only introduced above a threshold of approximately 2.5 GPa. In this way, we establish the capacity of gold nanocrystals to undergo complete pseudoelastic shape recovery following compression under moderate loads, as well as the onset of limited pseudoelastic behavior at higher loads. This work lays a foundation for future investigations of the limits of pseudoelastic deformation in a wide variety of metal nanocrystals.



INTRODUCTION

Over the last few decades, size-dependent mechanical behavior of metals has garnered increasing attention in the pursuit of higher performance materials. A wide variety of mechanical properties have been shown to vary with the size and crystalline structure at the nanoscale. Compression tests on nanowires and nanopillars gave rise to the "smaller is stronger" phenomenon, which showed face-centered cubic (fcc) metals like gold, silver and copper approach their theoretical strength with decreasing diameter^{1–3}. Young's modulus and bulk modulus have also shown to increase with decreasing size in nanowires^{4,5} and nanoparticles^{6,7}. These size-dependent properties have generally been attributed to either surface energy contributions that lead to lattice contraction^{4,7} or the altered density and nucleation of dislocations with decreased grain size^{2,8,9}. The changes in dislocation density and migration with increased surface accessibility lead to unique nanoscale deformation mechanisms, including brittle failure in typically ductile metals¹⁰ and dislocation-originated stacking fault tetrahedra¹¹.

One particularly interesting mechanical behavior recently reported to occur uniquely in nanoscale metals is pseudoelasticity^{12–15}. Pseudoelasticity refers to the ability to recover from large strains, far beyond the elastic limit of the metal. Classical pseudoelasticity occurs by phase transformations in shape memory alloys¹⁶, but recent studies report pseudoelastic shape recovery in the absence of phase transitions for very small (sub-10 nm diameter) gold and silver nanoparticles. In order to leverage these properties for the next generation of materials, it is critical to fully characterize their mechanical properties at the nanoscale, and that means overcoming their unique challenges.

Nanoscale materials, by virtue of the very length scales that impart their unique properties, present particular challenges with respect to measurement of their mechanical properties¹⁷. As a result, molecular dynamics simulations have been crucial to mechanistic understanding of nanoscale deformation ^{18–20}. However, the results from simulations are limited by idealized samples and testing conditions and require corroboration from experiments. Much of the existing experimental knowledge on size-dependent mechanical properties comes from nanoindentation^{21,22}, atomic force microscopy^{4,23} or *in situ* nanomechanical testing²⁴. While these experimental techniques offer powerful insights into local mechanical and deformation behavior, they suffer from uncertainty regarding the contributions of sample preparation²⁵, substrate effects²⁶ and, in the case of *in situ* electron microscopy measurements, electron beam effects^{24,27,28}. Additionally, most of the existing work has been performed on one-dimensional nanomaterials (nanowires or nanopillars)^{2-4,29}, while the size-dependent properties of other nanoscale geometries are less well-understood. We need experimental techniques to probe new sample configurations and environments in order to fully take advantage of their insights. Optical measurements allow for measurement on an ensemble of nanocrystals in the absence of surface effects and electron beam effects of concern in other methods.

The plasmon resonance of gold nanoparticles has been previously monitored by optical absorbance spectroscopy during compression in a diamond anvil cell^{13,30–35}. The effects observed in plasmonic nanoparticles under compression are attributed to a combination of changes in the dielectric function of the metal^{31,32,36,37}, changes in the refractive index of the pressure medium^{32,34,38,39}, changes in the crystallinity of the metal^{13,30,40–42}, and changes in the shape of the particles themselves^{13,30,40,43}. The relative contribution of each of these effects depends on the type of compression applied and the particles under investigation. For hydrostatic compression

of particles, shape change and plastic deformation are negligible, so the plasmon response is dominated by changes in the dielectric function of the metal and changes in the refractive index of the surroundings³². The sensitivity of the plasmon to the refractive index of the surrounding depends strongly on the size and shape of the nanoparticles, with larger, anisotropic particles exhibiting high sensitivity while smaller, spherical particles exhibit lower sensitivity to their surroundings^{44,45}.

Under non-hydrostatic compression of small, quasi-spherical particles, shape change and plastic deformation play the largest role in the response of the plasmon resonance. Recent studies of non-hydrostatic compression of small, quasi-spherical gold nanocrystals showed that a reversible red-shift of the plasmon resonance during compression indicates a reversible shape change, while an irreversible decrease in the absorbance efficiency was shown by electrodynamic simulations¹³ and x-ray diffraction⁴⁰ to indicate the introduction of crystalline defects. Intriguingly, while in situ mechanical testing of silver nanoparticles showed complete shape recovery and the absence of crystalline defects after compression¹², in these optical studies gold nanoparticles showed a limited pseudoelasticity: complete shape recovery accompanied by the introduction of long-lived crystalline defects¹³. This presents the exciting prospect that we can non-invasively monitor both the shape and plastic damage to the nanocrystals during compression. Here we take advantage of optical characterization of nanoparticle mechanics to explore the limits of pseudoelasticity in gold nanocrystals. We report that, while compression to high pressures results in limited pseudoelasticity in gold nanocrystals, after compression to moderate pressures full pseudoelastic shape recovery can occur without the introduction of longlived crystalline defects.

EXPERIMENTAL METHODS

Oleylamine-capped gold nanocrystals were synthesized by reduction of gold (III) chloride by *tert*-butylamine-borane complex in tetralin and oleylamine, as previously described⁴⁶. Following synthesis, the oleylamine was exchanged for 1-dodecanethiol by refluxing in toluene. The nanocrystals were cleaned by centrifugation and resuspended in toluene for further experiments. The nanocrystals were characterized by absorbance spectroscopy and transmission electron microscopy. The concentration of the nanocrystal solution was adjusted to target an absorbance of approximately 0.5 in the diamond anvil cell. The gold nanocrystals in toluene were loaded into a diamond anvil cell assembled with a pre-indented stainless steel gasket and ruby powder, and the entire assembly was sealed immediately to prevent evaporation. The pressure was increased and decreased by a screw-driven piston and, at each increase or decrease of pressure, the absorbance spectrum through the diamonds was collected on an inverted microscope coupled to an imaging spectrometer. The fluorescence spectrum of the ruby at each data point was also collected for pressure calibration. See supporting information for further details.

RESULTS AND DISCUSSION

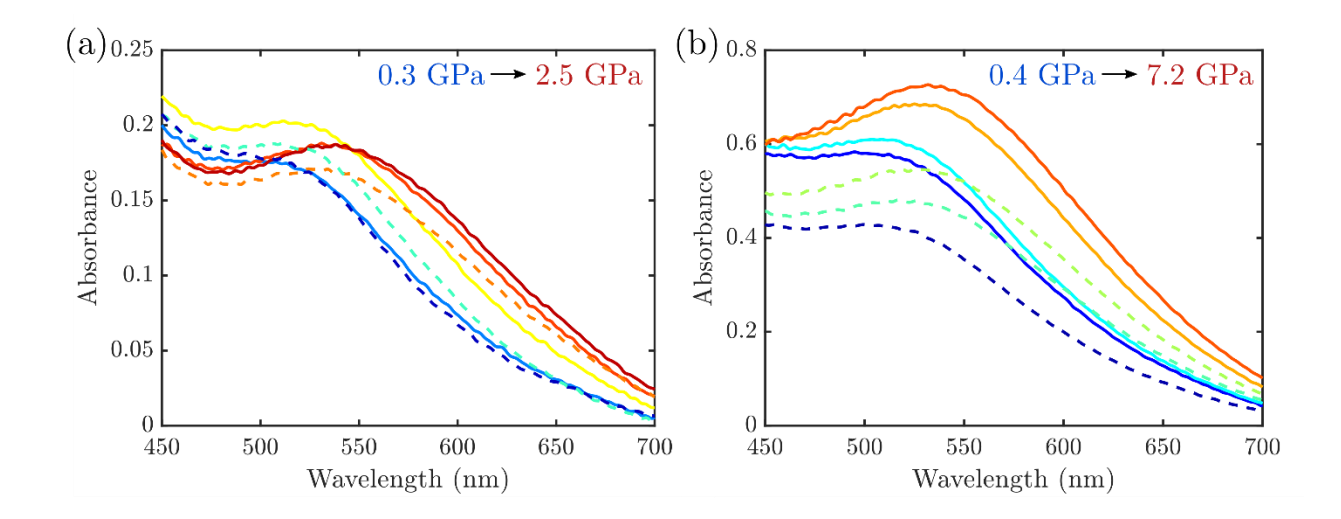


Figure 1. Absorbance spectra of gold nanoparticles under increasing (solid lines) and decreasing (dashed lines) non-hydrostatic compression. (a) Spectra during pressurization to 2.5 GPa. (b) Spectra during pressurization to 7.2 GPa. Spectra were smoothed with a low-pass filter for visualization.

Nanocrystals were synthesized according to previously reported methods⁴⁶ and characterized by UV/Vis absorbance spectroscopy and transmission electron microscopy (Figure S1). At ambient pressure in toluene, the particles exhibit a plasmon resonance at 505 nm (Supplementary Figure 1) that is in agreement with previous reports^{13,46} of approximately 4 nm diameter gold nanocrystals. Additionally, they exhibit a very low refractive index sensitivity, as tested by comparison of the absorbance spectra in toluene and hexane (Figure S1), again in accordance with previous reports of small, quasi-spherical gold particles^{45,47–49}. Transmission electron microscopy corroborates that average size of 4.4 nm and further shows a monodisperse, single population with a standard deviation of 0.6 nm (Figure S2).

The absorbance spectrum of the nanoparticles was collected while increasing and decreasing pressure in a diamond anvil cell (Figure 1). Toluene was used as a non-hydrostatic pressure medium⁵⁰. These experiments were repeated while varying the maximum pressure applied up to 11.4 GPa. Figure 1a shows an example series of spectra while increasing pressure to 2.5 GPa (solid lines) and while decreasing to ambient pressure (dotted lines). Figure 1b shows a similar example for compression to 7.2 GPa. In both cases, the plasmon resonance is seen to red-shift, a change which is reversible upon decompression. This change can be attributed to the shape change of the particles upon non-hydrostatic compression, which flattens the quasi-spherical particles into ellipsoids. While an ellipsoid should exhibit two plasmon modes, one red-shifted and one blue-shifted from the plasmon resonance of the sphere, the optical axis is aligned with the compression axis, so only the red-shifted mode is observed. In addition to the fully reversible red-shift, an irreversible decrease in the absorbance efficiency is seen after compression to 7.2 GPa. However, after compression to only 2.5 GPa, no irreversible decrease in absorbance efficiency is seen.

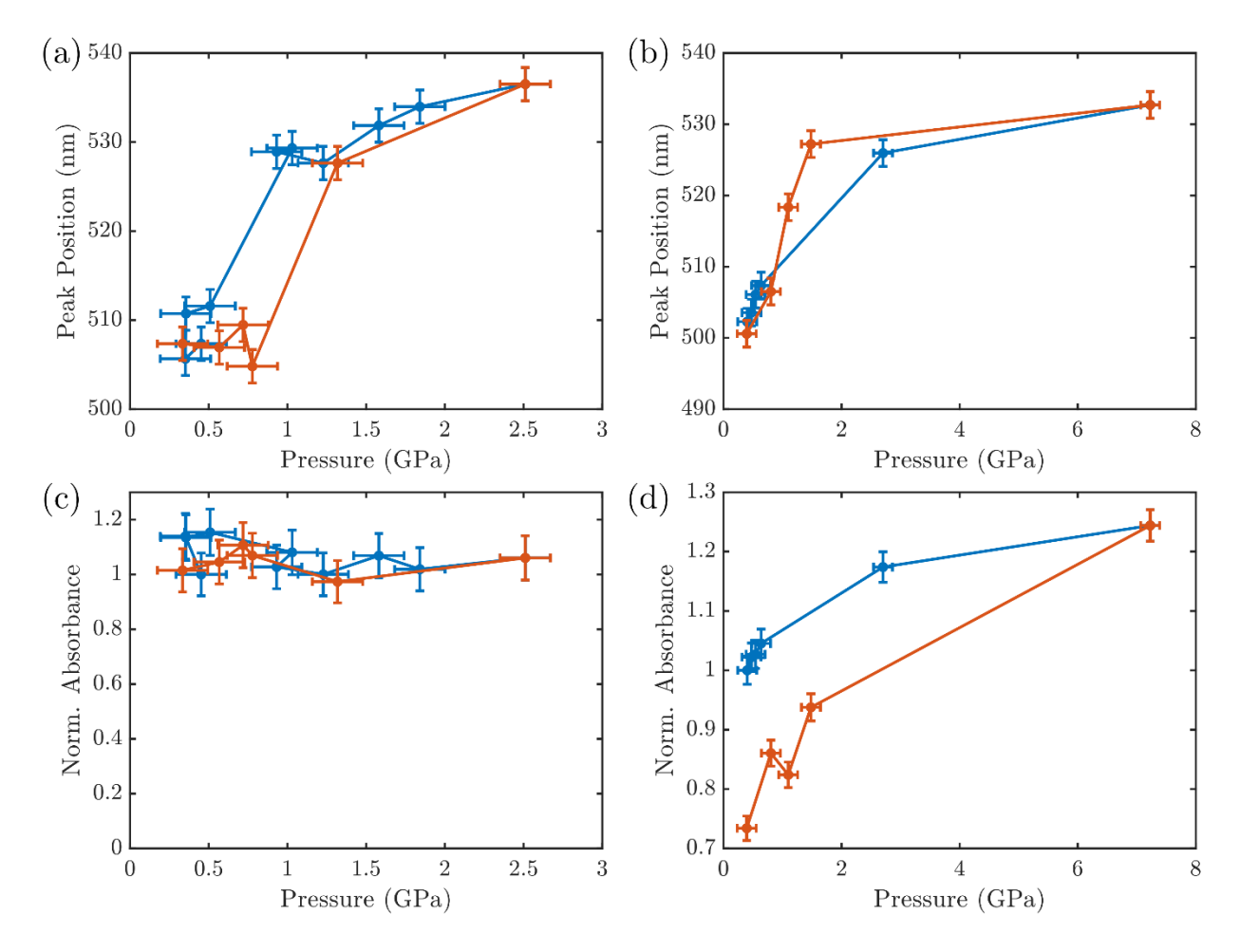


Figure 2. Peak position and absorbance efficiency under non-hydrostatic compression. (a) Peak position versus pressure up to 2.5 GPa. A rapid red-shift of approximately 30 nm is observed, which is reversible upon depressurization. (b) Peak position versus pressure up to 7.2 GPa. An initial, rapid red-shift of approximately 25 nm is observed, followed by a slower continued red-shift with further increase in pressure. (c) Absorbance at peak (normalized to initial peak absorbance) versus pressure up to 2.5 GPa. No change is observed. (d) Normalized peak absorbance versus pressure up to 7.2 GPa. An irreversible decrease in absorbance is observed upon depressurization.

Figure 2 shows the plasmon peak position (Figure 2a and 2b) and absorbance efficiency (Figure 2c and 2d) for the same two compression runs previously discussed, to maxima of 2.5 GPa and 7.2 GPa. As can be seen in Figure 2a, the peak position red-shifts rapidly from ambient pressure to approximately 2 GPa. The same behavior is observed in Figure 2b. However, upon further pressurization above 2 GPa, a slower continued red-shift is observed to the maximum pressure reached. In both cases, the peak position returns to its initial value after depressurization.

In contrast to the behavior of the peak position, however, the final absorbance efficiency does depend on the maximum pressures applied. When only pressurized to 2.5 GPa, no irreversible decrease in the absorbance efficiency was observed upon depressurization (Figure 2c). However, when pressurized to a maximum of 7.2 GPa, an irreversible decrease in absorbance efficiency was observed (Figure 2d). This example also shows the most common trajectory of absorbance efficiency during the pressurization run (Figure S3). The largest decreases in absorbance efficiency are seen over the same range in pressures as the shape change occurs, between 0 and 2.5 GPa.

The two cases discussed so far present two limiting cases of pseudoelastic shape recovery in gold nanoparticles. The first, when pressurized to moderate pressures, involves large, reversible shifts in plasmon resonance but no accompanying change in absorbance efficiency. The reversible peak shifts indicate complete shape recovery from large strains, while the absence of any irreversible decrease in absorbance efficiency indicates that no long-lived defects are introduced into the crystal as a result of the deformation. By contrast, following compression to higher pressures, complete shape recovery from large strains is still observed, in spite of an irreversible decrease in absorbance efficiency that indicates the introduction of damage to the crystal.

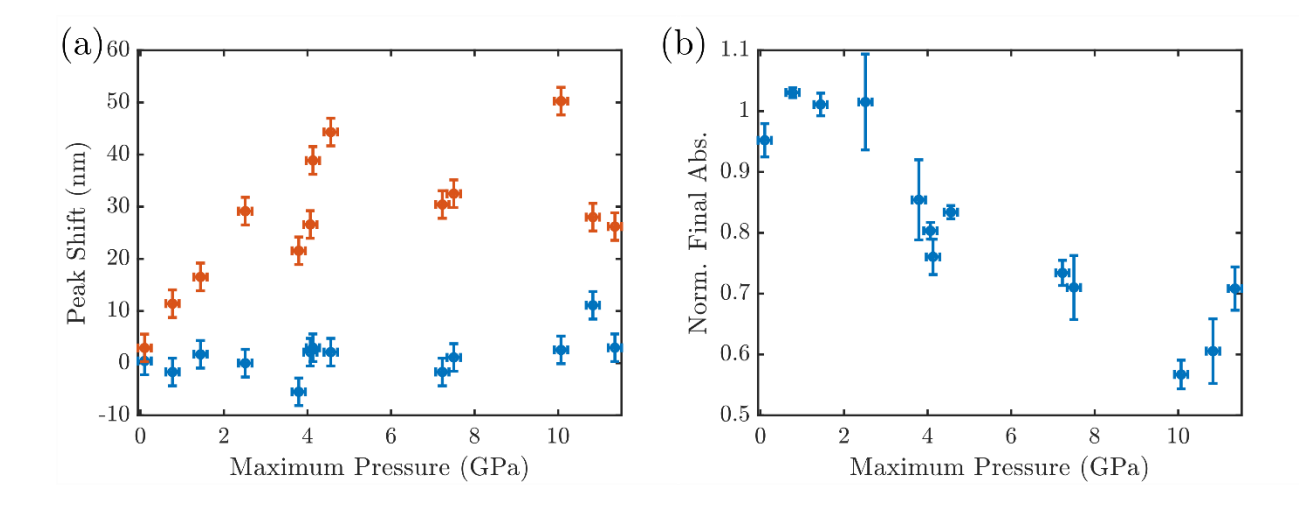


Figure 3. (a) Peak shift as a result of compression to varying maximum pressures. In red, shift at maximum applied pressure. In blue, shift after depressurization to ambient pressure. (b) Absorbance efficiency (normalized to the initial absorbance efficiency for each run) following compression to varying maximum pressures.

In order to examine the transition between these two cases, repeated experiments were performed to various maximum pressures between 0.1 GPa and 11.4 GPa. Figure 3a shows the relative shift of the plasmon resonance from its initial position at the maximum pressure applied (red circles) and at the final measurement following depressurization (blue circles). In all cases, the final peak position returns to its initial value, independent of pressure throughout the range, while the peak at the maximum applied pressure increases rapidly to approximately 2.5 GPa. Above 2.5 GPa no correlation is seen between maximum applied pressure and maximum shift, which varies between 20 nm and 50 nm red-shifted from the plasmon resonance at ambient pressure. The variation in the maximum observed shift is most likely due to variability in the differential stress generated in the DAC chamber, as has been seen in previous studies of non-hydrostatic

compression^{13,51,52} due to variation in gasket geometries⁵³ and the properties of the solid pressure medium.

It is worthwhile here to revisit the possible factors that contribute to the changes in plasmon resonance under pressure. Among the possible effects of pressure, refractive index changes in the solvent and changes in the dielectric function of the metal have relatively small effects on the plasmon resonance of small quasi-spherical nanocrystals, as confirmed in previous studies of quasi-hydrostatic compression of similar gold nanocrystals¹³. (See Figure S4 for a comparison of the predicted effect of refractive index changes in the solvent on the plasmon resonance with the observed shifts.) Coupling between plasmon resonances of neighboring particles has been avoided by controlling particle concentration to maintain average separations of several hundred nanometers⁵⁴, and there is no evidence of particle aggregation by brightfield microscopy of the diamond anvil cell chamber or transmission electron microscopy of nanocrystals recovered after compression (Figure S5). Furthermore, no correlation is observed between the particle concentration, as measured by the initial peak absorbance, and either the maximum observed shift or the final peak absorbance efficiency (Figure S6). Thus, we conclude that the shifts can be attributed to changes in particle shape, in agreement with previously published electrodynamic simulations¹³.

Interestingly, the final peak absorbance efficiency shows the opposite trend from that of the peak shift. Until a maximum applied pressure of approximately 2.5 GPa, no correlation is seen between the final peak absorbance efficiency (shown in Figure 3b, normalized to the initial peak absorbance) and the maximum applied pressure, and on average there is no change in the absorbance efficiency after pressurization. Above approximately 2.5 GPa, an increasingly large irreversible decrease in absorbance efficiency is seen with increasing maximum applied pressure.

As established in previous work by electrodynamic simulations¹³ and x-ray diffraction⁴⁰, the decrease in absorbance efficiency is caused by increased electron damping due to the introduction of crystalline defects to the nanocrystals. On the other hand, the peak position correlates directly to the overall shape of the particle. These measurements thus demonstrate the limitations of pseudoelastic deformation in these nanocrystals. Up to 2.5 GPa, deformation is pseudoelastic, with complete shape recovery from large strains without the introduction of long-lasting crystalline defects. On the other hand, above 2.5 GPa limited pseudoelasticity is seen, with complete shape recovery in spite of increasing damage to the crystal.

CONCLUSIONS

Pseudoelasticity in nanocrystals could be a key to design of reconfigurable or mechanically resilient materials that also take advantage of their other unique properties for electrical or optical functionality. This work establishes the possibility of that application through the first demonstration that pseudoelastic shape recovery can occur in gold nanocrystals without the introduction of long-lived crystalline damage. The lack of permanent damage to the crystal is important to the durability of any material or device that relies on this phenomenon.

Furthermore, we have established that the existence of a transition of completely pseudoelastic behavior to limited pseudoelastic behavior, in which shape recovery remains complete but crystalline damage is introduced. Future work will explore whether this property is also seen in other metal nanocrystals and over at what size regime it appears.

ASSOCIATED CONTENT

Supporting Information.

The following files are available free of charge.

Supplementary figures and methods (PDF): Additional experimental details and methods,

characterization of nanocrystals at ambient pressure before and after pressurization and pressure

dependence from repeated measurements.

AUTHOR INFORMATION

Corresponding Author

*Email: lindsey.hanson@trincoll.edu

Author Contributions

L.A.H. conceived of the project. L.A.H. and K.A.H. designed the experiments and data analysis.

L.A.H., K.A.H. and J.B. carried out the experiments. L.A.H. and J.B. wrote the manuscript.

ACKNOWLEDGMENT

The authors thank the National Science Foundation (DMR 2004867) and Trinity College

Summer Research Program for supporting this project. The authors declare no competing

financial interest.

REFERENCES

Uchic, M. D.; Dimiduk, D. M.; Florando, J. N.; Nix, W. D. Sample Dimensions Influence (1)

Strength and Crystal Plasticity. *Science*. **2004**, *305* (5686), 986–989.

(2) Greer, J. R.; De Hosson, J. T. M. Plasticity in Small-Sized Metallic Systems: Intrinsic versus

Extrinsic Size Effect. *Prog. Mater. Sci.* **2011**, *56* (6), 654–724.

(3) Greer, J. R.; Oliver, W. C.; Nix, W. D. Size Dependence of Mechanical Properties of Gold

14

- at the Micron Scale in the Absence of Strain Gradients. Acta Mater. 2005, 53, 1821–1830.
- (4) Cuenot, S.; Frétigny, C.; Demoustier-Champagne, S.; Nysten, B. Surface Tension Effect on the Mechanical Properties of Nanomaterials Measured by Atomic Force Microscopy. *Phys. Rev. B: Condens. Matter Mater. Phys.* **2004**, *69* (16), 1–5.
- (5) Jing, G. Y.; Duan, H. L.; Sun, X. M.; Zhang, Z. S.; Xu, J.; Li, Y. D.; Wang, J. X.; Yu, D. P. Surface Effects on Elastic Properties of Silver Nanowires: Contact Atomic-Force Microscopy. *Phys. Rev. B: Condens. Matter Mater. Phys.* 2006, 73 (23), 1–6.
- (6) Li, H.; Han, Y.; Duan, T.; Leifer, K. Size-Dependent Elasticity of Gold Nanoparticle Measured by Atomic Force Microscope Based Nanoindentation. *Appl. Phys. Lett.* 2019, 115 (5), 0–4.
- (7) Ouyang, G.; Zhu, W. G.; Sun, C. Q.; Zhu, Z. M.; Liao, S. Z. Atomistic Origin of Lattice Strain on Stiffness of Nanoparticles. *Phys. Chem. Chem. Phys.* **2010**, *12* (7), 1543–1549.
- (8) Greer, J. R.; Nix, W. D. Nanoscale Gold Pillars Strengthened through Dislocation Starvation. *Phys. Rev. B: Condens. Matter Mater. Phys.* **2006**, 73 (24), 1–6.
- (9) Flanagan, T. J.; Kovalenko, O.; Rabkin, E.; Lee, S. The Effect of Defects on Strength of Gold Microparticles. *Scr. Mater.* **2019**, *171*, 83–86.
- (10) Wang, J.; Sansoz, F.; Huang, J.; Liu, Y.; Sun, S.; Zhang, Z.; Mao, S. X. Near-Ideal Theoretical Strength in Gold Nanowires Containing Angstrom Scale Twins. *Nat. Commun.* 2013, 4, 1742.
- (11) Wei Wang, J.; Narayanan, S.; Yu Huang, J.; Zhang, Z.; Zhu, T.; Mao, S. X. Atomic-Scale

- Dynamic Process of Deformation-Induced Stacking Fault Tetrahedra in Gold Nanocrystals. *Nat. Commun.* **2013**, *4*, 2340.
- (12) Sun, J.; He, L.; Lo, Y.; Xu, T.; Bi, H.; Sun, L.; Zhang, Z.; Mao, S. X.; Li, J. Liquid-like Pseudoelasticity of Sub-10-Nm Crystalline Silver Particles. *Nat. Mater.* **2014**, *13*, 1007–1012.
- (13) Gu, X. W.; Hanson, L. A.; Eisler, C. N.; Koc, M. A.; Alivisatos, A. P. Pseudoelasticity at Large Strains in Au Nanocrystals. *Phys. Rev. Lett.* **2018**, *121* (5), 056102.
- (14) Wang, J.; Zeng, Z.; Weinberger, C. R.; Zhang, Z.; Zhu, T.; Mao, S. X. In Situ Atomic-Scale Observation of Twinning-Dominated Deformation in Nanoscale Body-Centred Cubic Tungsten. *Nat. Mater.* **2015**, *14* (6), 594–600.
- (15) Sharma, A.; Gazit, N.; Klinger, L.; Rabkin, E. Pseudoelasticity of Metal Nanoparticles Is Caused by Their Ultrahigh Strength. *Adv. Funct. Mater.* **2019**, 1807554.
- (16) Mohd Jani, J.; Leary, M.; Subic, A.; Gibson, M. A. A Review of Shape Memory Alloy Research, Applications and Opportunities. *Mater. Des.* **2014**, *56*, 1078–1113.
- (17) Richman, E. K.; Hutchison, J. E. The Nanomaterial Characterization Bottleneck. *ACS Nano* **2009**, *3* (9), 2441–2446.
- (18) Jiang, J. W.; Leach, A. M.; Gall, K.; Park, H. S.; Rabczuk, T. A Surface Stacking Fault Energy Approach to Predicting Defect Nucleation in Surface-Dominated Nanostructures. *J. Mech. Phys. Solids* **2013**, *61* (9), 1915–1934.
- (19) Bel Haj Salah, S.; Gerard, C.; Pizzagalli, L. Influence of Surface Atomic Structure on the

- Mechanical Response of Aluminum Nanospheres under Compression. *Comput. Mater. Sci.* **2017**, *129*, 273–278.
- (20) Valencia, F. J.; González, R. I.; Vega, H.; Ruestes, C.; Rogan, J.; Valdivia, J. A.; Bringa, E.
 M.; Kiwi, M. Mechanical Properties Obtained by Indentation of Hollow Pd Nanoparticles.
 J. Phys. Chem. C 2018, 122 (43), 25035–25042.
- (21) Mordehai, D.; Lee, S. W.; Backes, B.; Srolovitz, D. J.; Nix, W. D.; Rabkin, E. Size Effect in Compression of Single-Crystal Gold Microparticles. *Acta Mater.* **2011**, *59* (13), 5202–5215.
- (22) Bei, H.; Gao, Y. F.; Shim, S.; George, E. P.; Pharr, G. M. Strength Differences Arising from Homogeneous versus Heterogeneous Dislocation Nucleation. *Phys. Rev. B: Condens. Matter Mater. Phys.* **2008**, 77 (6), 2–5.
- (23) Kovalenko, O.; Rabkin, E. Mechano-Stimulated Equilibration of Gold Nanoparticles on Sapphire. *Scr. Mater.* **2015**, *107*, 149–152.
- (24) Wang, J.; Mao, S. X. Atomistic Perspective on in Situ Nanomechanics. *Extrem. Mech. Lett.*2016, 8, 127–139.
- (25) Kim, B. H.; Heo, J.; Kim, S.; Reboul, C. F.; Chun, H.; Kang, D.; Bae, H.; Hyun, H.; Lim, J.; Lee, H.; et al. Critical Differences in 3D Atomic Structure of Individual Ligand-Protected Nanocrystals in Solution. *Science*. 2020, 368 (6486), 60–67.
- (26) Wagner, R.; Moon, R.; Pratt, J.; Shaw, G.; Raman, A. Uncertainty Quantification in Nanomechanical Measurements Using the Atomic Force Microscope. *Nanotechnology*

- **2011**, 22 (45), 455703.
- (27) Sarkar, R.; Rentenberger, C.; Rajagopalan, J. Electron Beam Induced Artifacts during in Situ TEM Deformation of Nanostructured Metals. *Sci. Rep.* **2015**, *5*, 16345.
- (28) Zheng, H.; Cao, A.; Weinberger, C. R.; Huang, J. Y.; Du, K.; Wang, J.; Ma, Y.; Xia, Y.; Mao, S. X. Discrete Plasticity in Sub-10-Nm-Sized Gold Crystals. *Nat. Commun.* **2010**, *1*, 144.
- (29) Wang, L.; Liu, P.; Guan, P.; Yang, M.; Sun, J.; Cheng, Y.; Hirata, A.; Zhang, Z.; Ma, E.; Chen, M.; et al. In Situ Atomic-Scale Observation of Continuous and Reversible Lattice Deformation beyond the Elastic Limit. *Nat. Commun.* **2013**, *4*, 2413.
- (30) Bao, Y.; Zhao, B.; Tang, X.; Hou, D.; Cai, J.; Tang, S.; Liu, J.; Wang, F.; Cui, T. Tuning Surface Plasmon Resonance by the Plastic Deformation of Au Nanoparticles within a Diamond Anvil Cell. *Appl. Phys. Lett.* **2015**, *107* (20), 201909.
- (31) Bao, Y.; Zhao, B.; Hou, D.; Liu, J.; Wang, F.; Wang, X.; Cui, T. The Redshift of Surface Plasmon Resonance of Colloidal Gold Nanoparticles Induced by Pressure with Diamond Anvil Cell. *J. Appl. Phys.* **2014**, *115* (22), 223503.
- (32) Martin-Sanchez, C.; Barreda-Argueso, J. A.; Seibt, S.; Mulvaney, P.; Rodriguez, F. Effects of Hydrostatic Pressure on the Surface Plasmon Resonance of Gold Nanocrystals. *ACS Nano* **2019**, *13*, 498–504.
- (33) Barbillon, G. Nanoplasmonics in High Pressure Environment. *Photonics* **2020**, 7 (3), 53.
- (34) Martin-Sanchez, C.; Gonzalez-Rubio, G.; Mulvaney, P.; Guerrero-Martinez, A.; Liz-

- Marzan, L. M.; Rodriguez, F. Monodisperse Gold Nanorods for High-Pressure Refractive Index Sensing. *J. Phys. Chem. Lett.* **2019**, *10*, 1587–1593.
- (35) Medeghini, F.; Hettich, M.; Rouxel, R.; Silva Santos, S. D.; Hermelin, S.; Pertreux, E.; Torres Dias, A.; Legrand, F.; Maioli, P.; Crut, A.; et al. High-Pressure Effect on the Optical Extinction of a Single Gold Nanoparticle. *ACS Nano* **2018**, *12*, 10310–10316.
- (36) Mendoza-Cruz, R.; Parajuli, P.; Ojeda-Galván, H. J.; Rodríguez, Á. G.; Navarro-Contreras, H. R.; Velázquez-Salazar, J. J.; Bazán-Díaz, L.; José-Yacamán, M. Orthorhombic Distortion in Au Nanoparticles Induced by High Pressure. *CrystEngComm* 2019, 21 (22), 3451–3459.
- (37) Qian, X.; Park, H. S. The Influence of Mechanical Strain on the Optical Properties of Spherical Gold Nanoparticles. *J. Mech. Phys. Solids* **2010**, *58* (3), 330–345.
- (38) Martín-Sánchez, C.; Sánchez-Iglesias, A.; Mulvaney, P.; Liz-Marzán, L. M.; Rodríguez, F. Plasmonic Sensing of Refractive Index and Density in Methanol-Ethanol Mixtures at High Pressure. *J. Phys. Chem. C* **2020**, *124* (16), 8978–8983.
- (39) Runowski, M.; Sobczak, S.; Marciniak, J.; Bukalska, I.; Lis, S.; Katrusiak, A. Gold Nanorods as a High-Pressure Sensor of Phase Transitions and Refractive-Index Gauge. *Nanoscale* **2019**, *11* (18), 8718–8726.
- (40) Parakh, A.; Lee, S.; Harkins, K. A.; Kiani, M. T.; Doan, D.; Kunz, M.; Doran, A.; Hanson, L. A.; Ryu, S.; Gu, X. W. Nucleation of Dislocations in 3.9 Nm Nanocrystals at High Pressure. *Phys. Rev. Lett.* 2020, 124 (10), 106104.

- (41) Pileni, M. P. Impact of the Metallic Crystalline Structure on the Properties of Nanocrystals and Their Mesoscopic Assemblies. *Acc. Chem. Res.* **2017**, *50* (8), 1946–1955.
- (42) Yang, P.; Portalès, H.; Pilenia, M. P. Dependence of the Localized Surface Plasmon Resonance of Noble Metal Quasispherical Nanoparticles on Their Crystallinity-Related Morphologies. *J. Chem. Phys.* **2011**, *134* (2), 024507.
- (43) Ameer, F. S.; Varahagiri, S.; Benza, D. W.; Willett, D. R.; Wen, Y.; Wang, F.; Chumanov,
 G.; Anker, J. N. Tuning Localized Surface Plasmon Resonance Wavelengths of Silver
 Nanoparticles by Mechanical Deformation. J. Phys. Chem. C 2016, 120 (37), 20886–20895.
- (44) Willets, K. a; Van Duyne, R. P. Localized Surface Plasmon Resonance Spectroscopy and Sensing. *Annu. Rev. Phys. Chem.* **2007**, *58*, 267–297.
- (45) Chen, H.; Kou, X.; Yang, Z.; Ni, W.; Wang, J. Shape-and Size-Dependent Refractive Index Sensitivity of Gold Nanoparticles. *Langmuir* **2008**, *24*, 5233–5237.
- (46) Peng, S.; Lee, Y.; Wang, C.; Yin, H.; Dai, S.; Sun, S. A Facile Synthesis of Monodisperse Au Nanoparticles and Their Catalysis of CO Oxidation. *Nano Res.* **2008**, *I* (3), 229–234.
- (47) Lee, K.-S.; El-Sayed, M. A. Gold and Silver Nanoparticles in Sensing and Imaging: Sensitivity of Plasmon Response to Size, Shape, and Metal Composition. *J. Phys. Chem. B* **2006**, *110*, 19220–19225.
- (48) Miller, M. M.; Lazarides, A. A. Sensitivity of Metal Nanoparticle Surface Plasmon Resonance to the Dielectric Environment. *J. Opt. A Pure Appl. Opt.* **2006**, *8* (4), 21556–21565.

- (49) Khlebtsov, N. G.; Trachuk, L. A.; Mel'nikov, A. G. The Effect of the Size, Shape, and Structure of Metal Nanoparticles on the Dependence of Their Optical Properties on the Refractive Index of a Disperse Medium. *Opt. Spectrosc.* **2005**, *98* (1), 77–83.
- (50) Herbst, C.; Cook, R.; Jr, H. K. Density-Mediated Transport and the Glass Transition: High Pressure Viscosity Measurements in the Diamond Anvil Cell. *J. Non. Cryst. Solids* **1994**, *174*, 265–271.
- (51) Hemley, R. J.; Mao, H. K.; Shen, G.; Badro, J.; Gillet, P.; Hanfland, M.; Häusermann, D. X-Ray Imaging of Stress and Strain of Diamond, Iron, and Tungsten at Megabar Pressures. *Science*. **1997**, *276* (5316), 1242–1245.
- (52) Weidner, D. J.; Wang, Y.; Vaughan, M. T. Yield Strength at High Pressure and Temperature. *Geophys. Res. Lett.* **1994**, *21* (9), 753–756.
- (53) Dunstan, D. J. Theory of the Gasket in Diamond Anvil High-Pressure Cells. *Rev. Sci. Instrum.* **1989**, *60* (12), 3789–3795.
- (54) Jain, P. K.; Huang, W.; El-Sayed, M. A. On the Universal Scaling Behavior of the Distance Decay of Plasmon Coupling in Metal Nanoparticle Pairs: A Plasmon Ruler Equation. *Nano Lett.* 2007, 7 (7), 2080–2088.